PAPER • OPEN ACCESS

Adaptive Bayesian phase estimation for quantum error correcting codes

IOP Publishing New J. Phys. 21 (2019) 123027 https://doi.org/10.1088/1367-2630/ab5c51

New Journal of Physics
The open access journal at the forefront of physics

Deutsche Physikalische Gesellschaft DPG
IOP Institute of Physics

Published in partnership with: Deutsche Physikalische Gesellschaft and the Institute of Physics

OPEN ACCESS

RECEIVED
12 April 2019

REVISED
13 November 2019

ACCEPTED FOR PUBLICATION
27 November 2019

PUBLISHED
16 December 2019

PAPER

Adaptive Bayesian phase estimation for quantum error correcting codes

F Martínez-García[1], D Vodola[1,2,3] and M Müller[1,4,5]

[1] Department of Physics, Swansea University, Singleton Park, Swansea SA2 8PP, United Kingdom
[2] Dipartimento di Fisica e Astronomia dell'Università di Bologna, I-40127 Bologna, Italy
[3] INFN, Sezione di Bologna, I-40127 Bologna, Italy
[4] Institute for Quantum Information, RWTH Aachen University, D-52056 Aachen, Germany
[5] Peter Grünberg Institute, Theoretical Nanoelectronics, Forschungszentrum Jülich, D-52425 Jülich, Germany

E-mail: markus.muller@swansea.ac.uk **and** markus.mueller@fz-juelich.de

Keywords: Bayesian learning, adaptive techniques, quantum tomography, phase estimation, state reconstruction

Abstract

Realisation of experiments even on small and medium-scale quantum computers requires an optimisation of several parameters to achieve high-fidelity operations. As the size of the quantum register increases, the characterisation of quantum states becomes more difficult since the number of parameters to be measured grows as well and finding efficient observables in order to estimate the parameters of the model becomes a crucial task. Here we propose a method relying on application of Bayesian inference that can be used to determine systematic, unknown phase shifts of multi-qubit states. This method offers important advantages as compared to Ramsey-type protocols. First, application of Bayesian inference allows the selection of an adaptive basis for the measurements which yields the optimal amount of information about the phase shifts of the state. Secondly, this method can process the outcomes of different observables at the same time. This leads to a substantial decrease in the resources needed for the estimation of phases, speeding up the state characterisation and optimisation in experimental implementations. The proposed Bayesian inference method can be applied in various physical platforms that are currently used as quantum processors.

1. Introduction

Quantum computers have the potential to solve some computationally hard problems in a more efficient way than classical computers [1]. However, due to coupling with the environment, they are more susceptible than their classical counterparts to dynamical errors that affect the correct behaviour of the algorithms performed [2]. In order to cope with dynamical errors, quantum error correction techniques [3] need to be applied together with a correct initialisation of quantum states that, in general, suffers from different types of noise. These imperfections can often be modelled as irreversible couplings to the environment [4] or as unknown but constant unitary operations appearing due to systematic errors. Due to their constant nature, the latter can be compensated by determining the unknown operations and applying their inverse onto the state. The simplest instance of such systematic errors is given by single-qubit phase shifts which can transform a desired state $\alpha|0\rangle + \beta|1\rangle$ into $\alpha|0\rangle + \beta e^{i\phi}|1\rangle$ where ϕ is an unknown but constant phase. Estimates of this phase shift can be obtained by performing Ramsey-type experiments[5, 6] and, more recently, by adaptive methods based on application of Bayesian inference [7–15]. Most of these adaptive methods select the measurement to be performed by numerical optimisation of the information gained based on the results obtained in the previous measurements.

The characterisation of multi-qubit states, such as those needed for quantum error correcting codes [16], is a more complex problem. It is well known that quantum state tomography [17] becomes impractical to fully characterise these states since the resources needed scale exponentially with the number of qubits. Additionally, the systematic errors to be corrected can drift slowly over time. Thus, the error estimation process must be

performed on a time scale small enough so that, after the process yields an estimate of the error, the actual true value of the error has not shifted considerably compared to the uncertainty of the estimation process. As adaptive techniques can take advantage of experimental data collected at each measurement step, they can be successfully employed for increasing the information obtained with each measurement and thus decreasing the amount of resources and time needed as compared to non-adaptive techniques.

Along this line, in this work, we propose and explore an adaptive method based on the application of Bayesian inference for the characterisation of medium-scale multi-qubit states. For concreteness, we focus on the estimation of phases appearing in stabiliser states used in quantum error correction. We examine the efficiency of the method by studying the number of measurements needed and we derive an analytical rule to obtain the optimal measurement to perform at each time. This simple rule does not rely on numerical calculations and ensures the adaptiveness of the method to find the optimal measurement at each step. This renders the protocol particularly suitable for on-chip processing in adaptive control systems.

In addition, we evaluate the efficiency of our adaptive method and compare it to that of the phase optimisation method (PHOM), a non-adaptive phase estimation method developed in [18]. The latter method is based on a generalisation of a Ramsey experiment to determine and compensate systematic phases appearing in multi-qubit states and it was proposed and performed experimentally for the seven-qubit quantum error correcting colour code (Steane code) [19]. For this reason, we choose to evaluate the efficiency of our adaptive method for the phase characterisation of the states used for the Steane code and we show that our method has an improvement in the efficiency compared to the PHOM.

Remarkably, this adaptive method is not restricted only to the Steane code, but can be used for other multi-qubit states since it only relies on the application of simple single-qubit operations and measurements. As a consequence, the results shown in this paper are applicable to the optimisation of other QEC codes and the compensation of systematic errors appearing in other physical platforms for quantum-information processing such as, e.g. trapped ions [20–28], Rydberg atoms [29–31] in optical lattices [32–34] or tweezer arrays [35, 36] or other AMO or solid-state architectures [37–42].

This paper is organised as follows: in section 2 we introduce the concepts and notation for a one-qubit state phase measurement by using a Ramsey experiment and a Bayesian inference process. In section 3 we briefly review basic properties of the Steane code to which we will apply our technique. In section 4 we compare the efficiencies of the PHOM proposed in [18] and our Bayesian inference method to an intermediate quantum state obtained during the preparation of the logical states of the Steane code since this intermediate state has a less complex structure than the final states of the code. In section 5 we generalise the previous results and present a Bayesian inference method to estimate the phase shifts on the fully encoded seven-qubit logical states. Finally, in section 6 we summarise our results, especially the comparison between the results obtained for the efficiency of our method with the method in [18], and conclude with a brief outlook.

2. One qubit case

In this section, we will show how to estimate the unknown phase ϕ of the following quantum state

$$|\psi\rangle = \frac{1}{\sqrt{2}}(|0\rangle + e^{i\phi}|1\rangle) \tag{1}$$

from a finite set of data obtained from measurements. We suppose we can prepare as many copies of $|\psi\rangle$ as needed. Since measurements of the $\hat{Z}$ Pauli operator yield no information about ϕ we will perform measurements of the operator

$$\hat{O}_\theta = \cos(\theta)\hat{X} + \sin(\theta)\hat{Y} \tag{2}$$

on the XY plane of the Bloch sphere (see figure 1 (a)). Thus, the expected value of this operator for the state $|\psi\rangle$ is

$$\langle\psi|\ \hat{O}_\theta|\psi\rangle = \cos(\phi - \theta). \tag{3}$$

In the following, we will study two different ways in which we can select θ in equation (2) in order to obtain the value ϕ: Ramsey scan and a Bayesian inference process.

2.1. Ramsey scan

In order to estimate ϕ, one can apply a Ramsey-type experiment that can be summarised as follows (see figure 1): first we divide the interval $[-\pi, \pi)$ in M equidistant points

$$\theta_m = m \cdot \frac{2\pi}{M} - \pi, \quad m = 0, 1, \ldots, M-1. \tag{4}$$

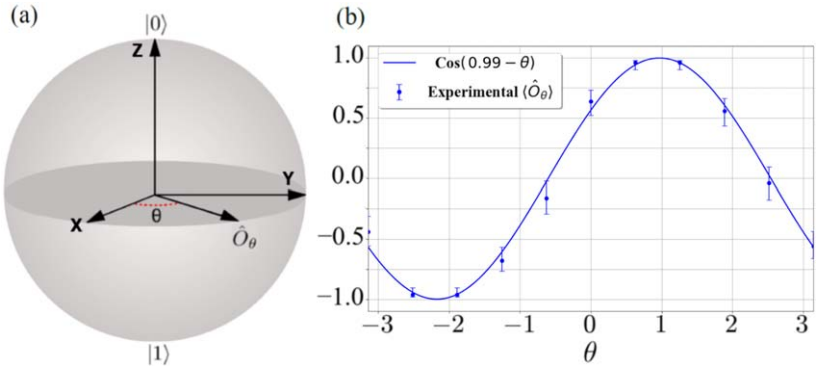

Figure 1. (a) Bloch sphere representation of the measurements to be performed for estimating the phase ϕ of the quantum state of equation (1). The observables $\hat{O}_\theta$ are obtained by rotating the observable $\hat{X}$ around the Z axis by an angle θ. The way $\hat{O}_\theta$ is selected depends on the method used to estimate ϕ. In the Ramsey scan case different values of θ are selected and several measurements are performed for each of these values. This allows a reconstruction of the expected sinusoidal dependence of $\langle\psi|\ \hat{O}_\theta|\psi\rangle$ with θ that yields an estimate for the phase ϕ (panel (b)). In the Bayes case, the outcomes of $\hat{O}_\theta$ are used to update the probability distribution $P(\phi)$. In this case, the value θ for each measurement is different and it is selected in a way that maximises the information gain per measurement (see section 2.2 and figure 2). (b) Ramsey scan simulation for the phase estimation of the state $|\psi\rangle$ in equation (1) with $\phi = 1$. The points represent the values $\hat{O}_{\theta_m}$ where the θ_m are $M = 10$ equidistant points in the interval $[-\pi, \pi)$. The points are obtained by simulating $N = 50$ measurements of $\hat{O}_{\theta_m}$ for each θ_m and they are used to fit a cosine whose phase A is the estimation obtained for ϕ and it is given by $A = 0.99 \pm 0.09$. The error of A is obtained by a bootstrap resampling [43].

For each of the values θ_m we estimate the expected value of $\hat{O}_{\theta_m}$ by $\langle\psi|\ \hat{O}_{\theta_m}|\psi\rangle = (N_+^{(m)} - N_-^{(m)})/N$ where $N_+^{(m)}$ ($N_-^{(m)}$) is the number of times we obtain a $+$ ($-$) when measuring in the $\hat{O}_{\theta_m}$ basis and N is the total number of measurements. Using the values $\langle\psi|\ \hat{O}_{\theta_m}|\psi\rangle$ obtained, we perform a least squares fit to a function of the form

$$f(\theta) = \cos(A - \theta), \tag{5}$$

where A is a phase. By comparison of equations (3) and (5), our estimate of ϕ is given by the fitted parameter A.

2.2. Bayesian inference

In this section we discuss how to use Bayes' theorem in order to estimate the value of ϕ. Bayes' theorem prescribes how to update the prior probability distribution of ϕ, $P(\phi)$, after a measurement $\mathcal{M}$ using its likelihood, $P(\mathcal{M}|\phi)$ (see figure 2). The final result is a posterior probability distribution of ϕ, $P(\phi|\mathcal{M})$, with the form

$$P(\phi|\mathcal{M}) \propto P(\mathcal{M}|\phi)P(\phi) \tag{6}$$

up to a normalisation factor. If we perform a new measurement we can apply Bayes' theorem again and use the obtained posterior as a prior for the next measurement and so on. For an increasing number of measurements the degree of uncertainty of ϕ will decrease, allowing us to reach a desired value in the uncertainty of the estimated value of ϕ. In our case we measure the operators $\hat{O}_\theta$ (with different values of θ for each measurement) with possible outcomes $+_\theta$ and $-_\theta$. The likelihoods of these outcomes for the state as given by equation (1) are

$$P(\pm_\theta|\phi) = \frac{1 \pm \cos(\phi - \theta)}{2}. \tag{7}$$

Assuming no prior knowledge about the value of ϕ we start with a uniform probability distribution $P(\phi) = 1/2\pi$ as a prior. After N measurements and applying equation (6) iteratively, the probability distribution for ϕ is given by

$$P(\phi|\pm_{\theta_1},\ldots,\pm_{\theta_N}) \propto P(\phi)P(\pm_{\theta_1}|\phi)\cdot\ldots\cdot P(\pm_{\theta_N}|\phi) = \frac{1}{2\pi}\cdot\frac{1 \pm \cos(\phi - \theta_1)}{2}\cdot\ldots\cdot\frac{1 \pm \cos(\phi - \theta_N)}{2}. \tag{8}$$

As the number of measurements increases, the posterior probability distribution can be approximated by a normal distribution with decreasing standard deviation.

2.2.1. Efficiency of the parameter learning process

In this section we show how the behaviour of the standard deviation of the distribution in equation (8) allows us to choose the value θ after each measurement in order to maximise the information gain of ϕ. It is expected that as we perform more measurements, the mean value of the probability distribution in equation (8) gets closer to the true value of ϕ and its standard deviation decreases. Let us suppose that, after a sufficiently large number n of measurements, the probability distribution $P_n(\phi)$ can be approximated by a Gaussian with mean $\bar{\phi}_n$ and standard deviation σ_n. For the measurement n, the probability $p_n^\pm$ of measuring $\pm$ when the angle selected is θ_n is

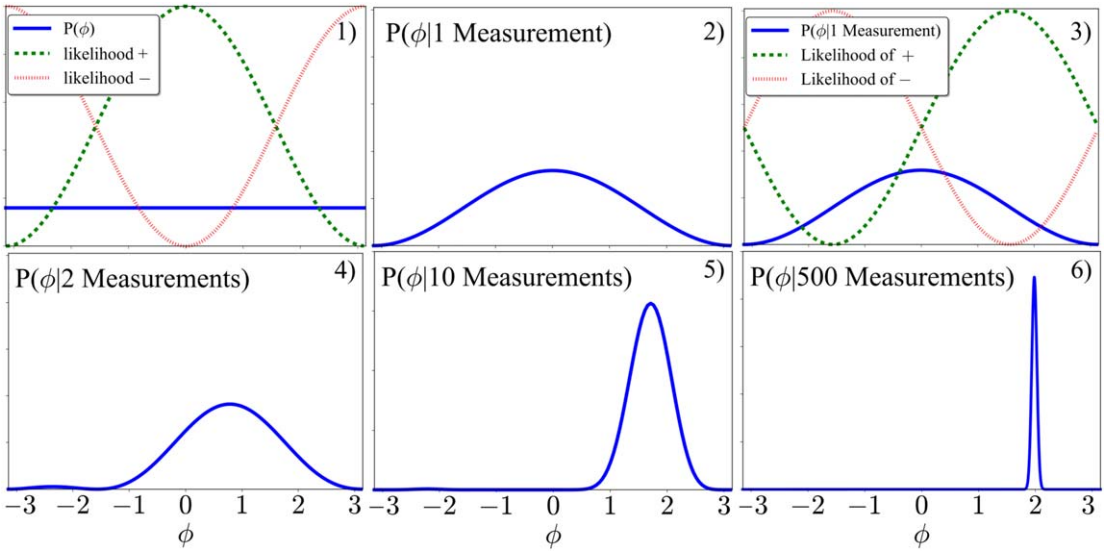

Figure 2. Bayesian inference process for the phase estimation of the state $|\psi\rangle$ in equation (1) with $\phi = 2$. Each step of the inference process consists in performing a measurement of the operator $\hat{O}_{\theta_{n-1}}$, updating the probability distribution based on the result of the measurement and selecting an optimal angle θ_n for the next measurement. (1) One starts with a uniform probability distribution of ϕ. $\theta = 0$ is selected for the first measurement. (2) If the + outcome is obtained (as assumed here), the probability distribution is updated by multiplying the prior probability distribution by the likelihood of obtaining a + and renormalizing. The maximum of $P(\phi|1\text{measurement})$ is located at $\phi = 0$. (3) The optimal selection of θ will be given by equation (13). Thus, we select $\theta = \pi/2$ for the next measurement. (4) Assume + is obtained again. The probability distribution can be updated again based on this result. This process of measuring, updating and finding the next optimal θ can be performed iteratively. (5) After 10 measurements the probability distribution can be approximated by a normal distribution. (6) After 500 measurements we obtain a normal distribution centred near the value $\phi = 2$ used for the simulation.

$$p_n^{\pm} = \int_{-\pi}^{\pi} \frac{1 \pm \cos(\phi - \theta_n)}{2} P_n(\phi)\,\mathrm{d}\phi. \tag{9}$$

The probability distribution after having obtained + or − is updated as

$$P_{n+1}^{\pm}(\phi) = \frac{1}{p_n^{\pm}} \frac{1 \pm \cos(\phi - \theta_n)}{2} P_n(\phi), \tag{10}$$

where $p_n^{\pm}$ appears due to normalisation. These posterior probability distributions will have a standard deviation denoted by $\sigma_{n+1}^{\pm}$. We obtain that the average decrease of the variance after performing measurement n is

$$\overline{\sigma_{n+1}^2 - \sigma_n^2} = -\alpha_n \sigma_n^4 \tag{11}$$

with

$$\alpha_n \equiv \frac{e^{\sigma_n^2} \sin^2(\overline{\phi}_n - \theta_n)}{1 - e^{\sigma_n^2} \cos^2(\overline{\phi}_n - \theta_n)}. \tag{12}$$

From an inspection of equations (11) and (12), we conclude that the maximum decrease on average for the variance is obtained when we select a value of θ_n that maximises the value of α_n. This is achieved (see figure 3) for

$$\theta_n = \overline{\phi}_n \pm \frac{\pi}{2}. \tag{13}$$

For this selection, the value of α_n approaches a constant value. Then, it can be proven that the succession in equation (11) has the following asymptotic solution:

$$\sigma_n^2 = \frac{1}{\alpha_n n}. \tag{14}$$

However, as the variance decreases, α_n approaches the constant value 1 (except for values close to $\theta_n = \overline{\phi}_n \pm k\pi$, $k \in \mathbb{N}$) as figure 3 shows. This means that after several measurements, the decrease of the variance will be independent on the value of θ we select for the next measurement and σ_n^2 will evolve as

$$\sigma_n^2 = \frac{1}{n}. \tag{15}$$

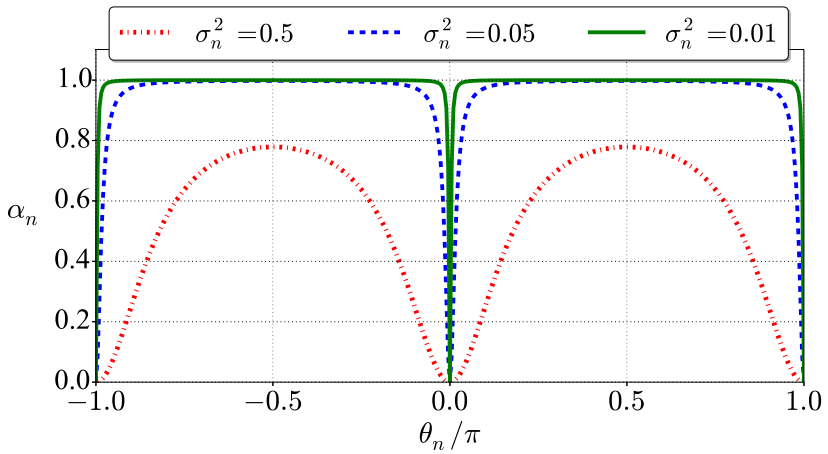

Figure 3. The quantity α dictates the decrease of the variance $\overline{\sigma_{n+1}^2 - \sigma_n^2}$ after each measurement step. This figure shows the dependence of α with θ_n for the case $\bar{\phi}_n = 0$ and different values of σ_n^2. Other values of $\bar{\phi}_n$ produce the same plot with a translation on the horizontal axis. As σ_n^2 decreases α approaches 1 except for the values $\theta = \bar{\phi}_n \pm k\pi$.

Similar results can be obtained by performing calculations involving Shannon's entropy [44] for the selection of the optimal measurement. However, this approach requires numerical calculations to obtain the optimal measurement in each step of the iteration. This increases the computational resources needed for *in situ* optimisation between experimental measurement runs as compared to the simple rule governed by equation (13) of our method. Figure 3 shows that after several measurements this adaptive way of selecting the next measurement becomes as efficient as a non-adaptive method for the one-qubit case. However, we stress that this is not a generic feature but specific to this simple example. In fact, we will show below that for the phase measurement of multi-qubit states an adaptive approach to the selection of the measurements yields an improvement in the efficiency as compared to the non-adaptive approach. It is worth mentioning that the result in equation (15) indicates that our increase in the knowledge of the system satisfies the standard quantum limit (SQL).

3. Characterisation of multi-qubit states

In quantum error correction the quantum information is encoded in entangled many-qubit systems. This provides protection against noise.

In the following sections we will discuss the estimation of systematic errors appearing in the preparation of the stabiliser states used in quantum error correction. For concreteness, we focus on the states used for the seven-qubit Steane code [19]. This code represents the minimal instance of 2D colour codes [45] and it is obtained by restricting a the Hilbert space of seven qubits to the subspace of states which are simultaneous $+1$ eigenstates of six commuting stabiliser operators $S_x^{(i)}$ and $S_z^{(i)}$, $i = 1, 2, 3$ (see figure 4). These stabilisers define a two-dimensional subspace for this seven-qubit system that can be used to encode a logical qubit. Additionally, the logical X and Z operators can be chosen as $X_L = \prod_{i=1}^{7} X_i$ and $Z_L = \prod_{i=1}^{7} Z_i$. The logical state $|0\rangle_L$ is defined by $Z_L\,|0\rangle_L = |0\rangle_L$

$$|0\rangle_L \propto (1 + Z_L)\prod_{i=1}^{3}(1 + S_x^{(i)})|0\rangle^{\otimes 7}. \tag{16}$$

Similarly, the logical $|1\rangle_L$ is defined by $Z_L\,|1\rangle_L = -|1\rangle_L$. These states satisfy $|1\rangle_L = X_L\,|0\rangle_L$ and $|0\rangle_L = X_L\,|1\rangle_L$.

However, due to imperfections during the initial state preparation of, for example, $|0\rangle_L$ in the experimental realisation of this code in [26], the obtained state will differ from the expected ideal one: on the one hand, dynamical phase shifts during the encoding sequence can accumulate and give rise to unknown, though systematic relative phases between the eight components of the expected ideal final state as given by equation (16), resulting instead in a state

$$\begin{aligned}|0'\rangle_L = \frac{1}{2\sqrt{2}}(&|0000000\rangle + e^{i\phi_1}|0110110\rangle + e^{i\phi_2}|1111000\rangle + e^{i\phi_3}|1001110\rangle \\ &+ e^{i\phi_4}|0011011\rangle + e^{i\phi_5}|0101101\rangle + e^{i\phi_6}|1100011\rangle + e^{i\phi_7}|1010101\rangle).\end{aligned} \tag{17}$$

Additionally, other errors and in particular incoherent processes can also generate population in additional states. A simple one-parameter model of such such state, ρ, which includes these possible errors is given by a

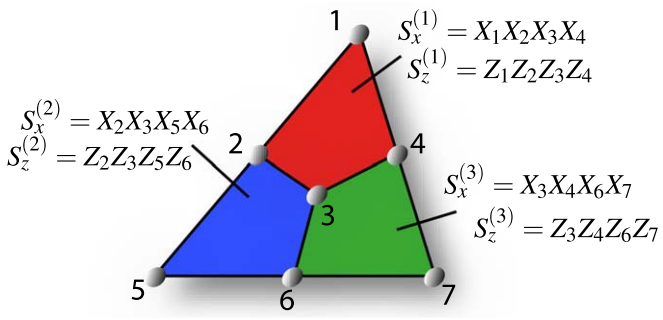

Figure 4. Steane code or seven-qubit colour code: a structure composed of seven qubits is used for encoding one logical qubit. The code is defined by six stabiliser generators $S_X^{(j)}$ and $S_Z^{(j)}$ for $j = 1, 2, 3$ associated with each of the four-qubit plaquettes. The code space is defined as the simultaneous $+1$ eigenspace of these stabilisers.

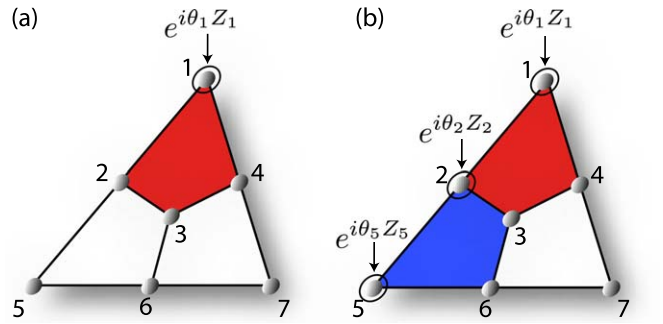

Figure 5. (a) One-plaquette case. During the first step of the preparation of the seven-qubit error correcting code, four-qubit entangling operations are performed on qubits 1–4. A phase appearing in the resulting state due to systematic errors can be estimated by performing measurements of $S_x^{(1)}$ for different rotations on the first qubit. This is similar to the single-qubit phase estimation. (b) Two-plaquette case. After the manipulation of the first and second plaquettes, up to three relative phases can appear in quantum state obtained. To estimate these phases we can perform measurements of $S_x^{(1)}$, $S_x^{(2)}$ and $S_x^{(1)}S_x^{(2)}$ for different rotations on the first, second and fifth qubit.

Werner-state of the form

$$\rho = \frac{p}{\dim}\mathbb{1} + (1 - p)|0'\rangle_L\langle 0'|_L, \tag{18}$$

where the first component represents a completely mixed state ($\dim = 2^7 = 128$ in our case). The parameter $p \in [0, 1]$ quantifies the magnitude of this white-noise component. For more experimental details on the origin of these errors we refer the interested reader to [18, 26].

We note that incoherent errors such as the one described by the mixed-state contribution in state (18) cannot be corrected by the techniques we discuss here. Therefore, to keep notation simple, in what follows we will omit the mixed state component in state descriptions and only consider the part of the state containing the relative phases which can be detected and compensated by the methods discussed. In the following sections we develop a method to measure these relative phases. As an introductory example, we will first study an intermediate state of the full seven-qubit Steane encoding process (two-plaquette case) to introduce the concepts that will be needed to correct the phases appearing in the fully encoded system (three-plaquette case).

4. Two-plaquette case

At the start of the preparation of the seven-qubit quantum error correcting code, four-qubit entanglement operations are applied to the first plaquette (figure 5 (a)). This yields the quantum state $|\psi_1\rangle \propto (1 + S_x^{(1)})|0\rangle^{\otimes 7}$ composed by the superposition of two components in the computational basis which can have a relative phase due to systematic errors. This is equivalent to a single-qubit phase estimation, as the phase can be corrected by rotating one of the four qubits and performing measurements of the $S_x^{(1)}$ stabiliser.

Therefore, we consider the state $|\psi_2\rangle$ obtained by application of four-qubit entangling operations to the first and second plaquettes (see figure 5 (b))

$$|\psi_2\rangle \propto (1 + S_x^{(1)})(1 + S_x^{(2)})|0\rangle^{\otimes 7}. \tag{19}$$

This state maximises the mean value of the X-type stabilisers on the first and second plaquette, $S_x^{(1)} = X_1X_2X_3X_4$, $S_x^{(2)} = X_2X_3X_5X_6$ and the product of both, $S_x^{(1)}S_x^{(2)} = X_1X_4X_5X_6$:

$$\langle\psi_2|\ S_x^{(1)}|\psi_2\rangle = \langle\psi_2|\ S_x^{(2)}|\psi_2\rangle = \langle\psi_2|\ S_x^{(1)}S_x^{(2)}|\psi_2\rangle = 1. \tag{20}$$

However, systematic phase shifts accumulate during the preparation of $|\psi_2\rangle$ due to experimental errors. The state $|\psi_2'\rangle$ containing these unknown phase shifts is

$$|\psi_2'\rangle \propto |0000000\rangle + e^{i\phi_1}|0110110\rangle + e^{i\phi_2}|1111000\rangle + e^{i\phi_3}|1001110\rangle. \tag{21}$$

In order to compensate these relative phase shifts we can apply single qubit Z rotations (see figure 5(b)). For example, by rotating the first, second and fifth qubits we obtain

$$\begin{aligned} e^{i\theta_1 Z_1}e^{i\theta_2 Z_2}e^{i\theta_5 Z_5}|\psi_2'\rangle \propto\ & |0000000\rangle + e^{i[\phi_1+2(\theta_2+\theta_5)]}|0110110\rangle \\ & + e^{i[\phi_2+2(\theta_1+\theta_2)]}|1111000\rangle + e^{i[\phi_3+2(\theta_1+\theta_5)]}|1001110\rangle. \end{aligned} \tag{22}$$

The selection of qubits to be rotated is arbitrary as long as these three rotations do not commute with $S_x^{(1)}$, $S_x^{(2)}$ and $S_x^{(1)}S_x^{(2)}$, respectively. The expected values of the stabilisers for the state in equation (22) are given by

$$\langle S_x^{(1)}\rangle = \frac{\cos[\phi_2 + 2(\theta_2 + \theta_1)] + \cos[\phi_1 - \phi_3 + 2(\theta_2 - \theta_1)]}{2}, \tag{23}$$

$$\langle S_x^{(2)}\rangle = \frac{\cos[\phi_1 + 2(\theta_2 + \theta_5)] + \cos[\phi_2 - \phi_3 + 2(\theta_2 - \theta_5)]}{2}, \tag{24}$$

$$\langle S_x^{(1)}S_x^{(2)}\rangle = \frac{\cos[\phi_3 + 2(\theta_5 + \theta_1)] + \cos[\phi_1 - \phi_2 + 2(\theta_5 - \theta_1)]}{2}, \tag{25}$$

In order to obtain information about the unknown systematic phases, we can perform measurements of these stabilisers for different values of the rotation angles θ. Once the values of these phases are measured it is possible to perform single-qubit rotations to transform the state $|\psi_2'\rangle$ into the desired state $|\psi_2\rangle$. A way to obtain these values is the PHOM [18]. We propose another method based on application of Bayesian inference. In the following subsections we review the PHOM and introduce our Bayesian protocol.

4.1. Phase optimisation method

The PHOM introduced in [18] is given by the following iterative protocol. For concreteness, here we review how it works for the optimisation of the state in equation (21).

(i) For each stabiliser, an associated rotation on a qubit i, θ_i, is chosen. The selection is arbitrary, but each stabiliser must not commute with its associated qubit rotation. We associate θ_2 with $S_x^{(1)}$, θ_5 with $S_x^{(2)}$ and θ_1 with $S_x^{(1)}S_x^{(2)}$.

(ii) Choose an initial configuration for the set of rotation parameters $\boldsymbol{\theta}^{(0)} = \{\theta_1^{(0)}, \theta_2^{(0)}, \theta_5^{(0)}\}$.

(iii) Scan $\langle S_x^{(1)}\rangle$ in a similar way as in the single-qubit case (see figure 1(b)) over its associated angle, θ_2, in the interval $[-\pi, \pi]$ while keeping $\theta_1 = \theta_1^{(0)}$ and $\theta_5 = \theta_5^{(0)}$ fixed. Determine and fix θ_2 to the value $\theta_2 = \theta_2^{(1)}$ for which $\langle S_x^{(1)}\rangle$ is maximised. Similarly perform scans of $\langle S_x^{(2)}\rangle$ over θ_5 to obtain $\theta_5^{(1)}$ and $\langle S_x^{(1)}S_x^{(2)}\rangle$ over θ_1 to obtain $\theta_1^{(1)}$. With these steps $\boldsymbol{\theta}^{(0)} = \{\theta_1^{(0)}, \theta_2^{(0)}, \theta_5^{(0)}\}$ has changed to $\boldsymbol{\theta}^{(1)} = \{\theta_1^{(1)}, \theta_2^{(1)}, \theta_5^{(1)}\}$. Performing this step completes one PHOM iteration.

(iv) The values of the angles $\boldsymbol{\theta}$ might not converge to the values that correct the phases after only one iteration. Thus, repeat step (iii) for a number of iterations I until the set of angles $\boldsymbol{\theta}$ converges to a desired precision.

This method gives an estimate of the angles θ_1, θ_2 and θ_5 that correct the systematic phases ϕ_1, ϕ_2 and ϕ_3. The precision of this estimate will become better as the number of measurements used for the scans increases. In this work we also introduce a variation of this PHOM to measure phases that we call the constant cosine PHOM.

4.1.1. Constant cosine PHOM

The constant cosine PHOM is a similar method that also performs scans of the expected values of the stabilisers for different qubit rotations to obtain a correction for systematic phases. This process is more similar to a Ramsey experiment as only one scan of each stabiliser is needed. From equation (23) we can see that, if we keep the value $\theta_2 - \theta_1$ fixed and vary $\theta_2 + \theta_1$, the mean value of $\langle S_x^{(1)}\rangle$ will be given by

$$\langle S_x^{(1)}\rangle = \frac{\cos[\phi_2 + 2(\theta_2 + \theta_1)] + h}{2}, \quad h \equiv \cos[\phi_1 - \phi_3 + 2(\theta_2 - \theta_1)], \tag{26}$$

where h is constant for all the measurements since the difference $\theta_2 - \theta_1$ is fixed. Thus the angle ϕ_2 that represents the phase shift to be corrected is given by the value of $-2(\theta_2 + \theta_1)$ for which a maximum in the mean value $\langle S_x^{(1)}\rangle$ is reached. By analysing $\langle S_x^{(2)}\rangle$ and $\langle S_x^{(1)} S_x^{(2)}\rangle$ in a similar way one can then obtain ϕ_1 and ϕ_3, too.

4.2. Bayesian inference method

In the following we will introduce and analyse two Bayesian inference methods to measure the phases in the state $|\psi_2'\rangle$ of equation (21) of the two-plaquette case. These methods are (i) a Bayesian inference method by direct application of the likelihoods, and (ii) a Bayesian inference method using marginal likelihoods. We will first describe this direct Bayesian inference method and then explain the method we propose to improve the PHOM, namely the marginal likelihood method.

4.2.1. Direct Bayesian inference method

An estimation of the phases using Bayesian inference is performed by measuring the plaquettes and updating the probability distribution based on the results obtained. The likelihoods for each plaquette measurement can be obtained from the expressions for the expected values by

$$P_1(\pm_{\boldsymbol{\theta}}|\boldsymbol{\phi}) = \frac{1 \pm \langle S_x^{(1)}\rangle}{2}, \quad P_2(\pm_{\boldsymbol{\theta}}|\boldsymbol{\phi}) = \frac{1 \pm \langle S_x^{(2)}\rangle}{2}, \quad P_{12}(\pm_{\boldsymbol{\theta}}|\boldsymbol{\phi}) = \frac{1 \pm \langle S_x^{(1)} S_x^{(2)}\rangle}{2}, \tag{27}$$

where $P_1(\pm_{\boldsymbol{\theta}}|\boldsymbol{\phi})$ is the likelihood of obtaining a $+$ or a $-$ outcome when measuring $S_x^{(1)}$ for $\boldsymbol{\theta} = \{\theta_1, \theta_2, \theta_5\}$ and $\boldsymbol{\phi} = \{\phi_1, \phi_2, \phi_3\}$. Similarly, $P_2(\pm_{\boldsymbol{\theta}}|\boldsymbol{\phi})$ is related to $S_x^{(2)}$ and $P_{12}(\pm_{\boldsymbol{\theta}}|\boldsymbol{\phi})$ to $S_x^{(1)} S_x^{(2)}$. For instance, the likelihood for $S_x^{(1)}$ is given by

$$P_1(\pm_{\boldsymbol{\theta}}|\boldsymbol{\phi}) = \frac{2 \pm \cos[\phi_2 + 2(\theta_2 + \theta_1)] \pm \cos[\phi_1 - \phi_3 + 2(\theta_2 - \theta_1)]}{4}. \tag{28}$$

Since the likelihoods used are functions of three variables, the obtained probability distribution will be a three-dimensional function. In general, if the number of unknown parameters appearing in the likelihoods of the experiment increases, the probability distribution obtained will be a function of many variables and, therefore, finding the most probable values for the phases and their variance becomes more difficult. This complication can be avoided if in the measurement of each stabiliser we keep one of the cosines constant in a similar way as it is done for the constant cosine PHOM. This yields a likelihood given by (see also equation (26))

$$P_1(\pm_{\boldsymbol{\theta}}|\phi_2, h) = \frac{2 \pm h_2 \pm \cos[\phi_2 + 2(\theta_2 + \theta_1)]}{4} \tag{29}$$

for the first plaquette, where the value $\theta_2 - \theta_1$ is kept constant to ensure that one of the cosines has a constant value given by h_2. Similar expressions can be obtained for the other stabilisers. This approach yields normal probability distributions defined on two variables, one being h_1, h_2 or h_3 and the other being ϕ_1, ϕ_2 or ϕ_3 depending on the stabiliser that is measured. The estimate for each phase is easily obtained from its corresponding probability distribution.

We now numerically compare this method and the constant cosine PHOM protocol (see figure 6). Performing a fit of the numerical data we obtain that for the PHOM the scaling of the variance as a function of the number of measurements n is given by $\sigma_{i,n}^2 = (6.6 \pm 0.2)/n$ when estimating the single angle ϕ_i. Similarly, for the constant cosine Bayes we obtain $\sigma_{i,n}^2 = (6.2 \pm 0.6)/n$. However, in order to obtain an estimate of the other two phases, this process must be repeated for each of the other stabilisers. This yields a scaling of the variance of $\sigma_n^2 = (19.8 \pm 0.4)/n$ for the PHOM and $\sigma_n^2 = (18.6 \pm 1.0)/n$ for the constant cosine Bayes method. This provides an estimate of the efficiency of the PHOM and the direct Bayesian inference method for the intermediate state $|\psi_2'\rangle$.

In the following, we will introduce and analyse the Bayesian marginal likelihood method, which provides an improvement in efficiency over both the PHOM and the constant cosine Bayesian inference method.

4.2.2. Marginal likelihood method

Let us first consider measurements of the first stabiliser whose likelihood is given by

$$P_1(\pm_{\boldsymbol{\theta}}|\boldsymbol{\phi}) = \frac{2 \pm \cos[\phi_2 + 2(\theta_2 + \theta_1)] \pm \cos[\phi_1 - \phi_3 + 2(\theta_2 - \theta_1)]}{4}. \tag{30}$$

Let us for the moment focus on measuring the value of ϕ_2. To estimate this phase, we have two different control parameters, θ_1 and θ_2, that we can change before each measurement. We choose to perform a measurement under the constraint of keeping the value of $2(\theta_2 - \theta_1)$ fixed to a certain value θ_c while changing the value of $2(\theta_2 + \theta_1)$. With this choice the argument of the cosine containing $\phi_1 - \phi_3$ is fixed and this cosine term assumes a constant value c_2. This yields the following likelihood

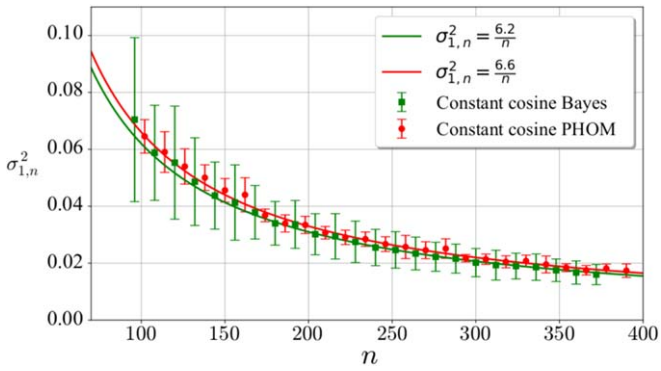

Figure 6. Behaviour of the variance of ϕ_1 obtained for the simulations of the constant cosine approach for both the PHOM (red circles) and the Bayesian inference (green squares) as a function of the number of measurements n. Solid lines represent fits of the numerical data obtained for both methods. The same behaviour is obtained for ϕ_2 and ϕ_3 (not shown).

$$P_1(\pm_{\theta}|\phi_2) = \frac{2 \pm \cos[\phi_2 + 2(\theta_2 + \theta_1)] \pm c_2}{4}. \tag{31}$$

Now, for a second measurement we select θ_1 and θ_2 values such that they fulfil the same constraint as before but shifted by $\pm\pi$, i.e. $2(\theta_2 - \theta_1) = \theta_c \pm \pi$. For this selection, the value of the second cosine term in equation (30) becomes $-c_2$ instead of c_2 and the likelihood will be given by

$$P_1(\pm_{\theta}|\phi_2) = \frac{2 \pm \cos[\phi_2 + 2(\theta_2 + \theta_1)] \mp c_2}{4}. \tag{32}$$

Therefore, if we fix $2(\theta_2 + \theta_1)$ and perform such a combined pair of measurements under the discussed constraints, one with c_2 and another with $-c_2$, we can marginalise over c_2 to obtain the following marginal likelihood for each individual measurement

$$P_1(\pm_{\theta}|\phi_2) = \frac{2 \pm \cos[\phi_2 + 2(\theta_2 + \theta_1)]}{4}, \tag{33}$$

which only depends on ϕ_2. After this pair of measurements, we then fix $2(\theta_2 + \theta_1)$ to a new value and perform another pair of measurements in the same way as before. The key observation is that, as a result of this process, the likelihood obtained is similar to the one for the single qubit case of equation (7). This allows one to directly generalise the analysis for the scaling of the variance for ϕ_2 (see equation (11) and appendix B) obtaining

$$\overline{\sigma^2_{2,n+1} - \sigma^2_{2,n}} = -\alpha_{2,n}\sigma^4_{2,n}, \tag{34}$$

where

$$\alpha_{2,n} \equiv \frac{\exp(\sigma^2_{2,n})\sin^2(\overline{\phi}_{2,n} - \tilde{\theta}_{2,n})}{4 - \exp(\sigma^2_{2,n})\cos^2(\overline{\phi}_{2,n} - \tilde{\theta}_{2,n})}, \tag{35}$$

and $\tilde{\theta}_{2,n} \equiv -2(\theta_{2,n} + \theta_{1,n})$. For small values of $\sigma^2_{2,n}$, $\alpha_{2,n}$ can be approximated by (see figure 7)

$$\alpha_{2,n} \approx \frac{\sin^2(\overline{\phi}_{2,n} - \tilde{\theta}_{2,n})}{4 - \cos^2(\overline{\phi}_{2,n} - \tilde{\theta}_{2,n})}. \tag{36}$$

Note that in this two-plaquette case, in equation (36) a 4 appears in the denominator, as opposed to the 1 appearing in the one-qubit case. Due to this, the quantity $\alpha_{2,n}$, which determines the decrease in the uncertainty, has a sinusoidal behaviour between 0 and 1/4. Note also that in constrast to the single-qubit case (see figure 3) this oscillatory behaviour does not disappear with an increasing number of measurements. Figure 7 shows that the decrease in the standard deviation is maximised if we choose $\tilde{\theta}_{2,n} = \bar{\phi}_{2,n} \pm \pi/2$, making this the optimal adaptive measurement selection. For this optimal choice the value of $\alpha_{2,n}$ is 1/4 and accordingly the variance scales as $\sigma^2_{2,n} = 4/n$.

So far, in the explanation of the protocol we have focused on estimating ϕ_2. However, our protocol allows one to measure ϕ_1, ϕ_2 and ϕ_3 at the same time. Based on the adaptive way of selecting the measurements as explained above, we make the following selection

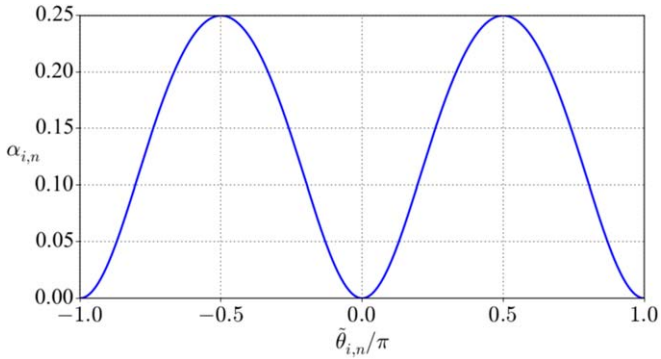

Figure 7. Dependence of the factor $\alpha_{i,n}$ on $\tilde{\theta}_{i,n}$ for $i = 1, 2, 3$ (here $\bar{\phi}_{i,n} = 0$). $\alpha_{i,n}$ dictates the decrease of the variance step by step. $\alpha_{i,n}$ oscillates between 0 and 0.25 and its mean value is $(2 - \sqrt{3})/2 \approx 0.134$, with its maximum at $\tilde{\theta}_{i,n} = \bar{\phi}_{i,n} \pm \pi/2$. By equation (14), this is the optimal way of selecting $\tilde{\theta}_{i,n}$.

$$\begin{cases} \tilde{\theta}_{1,n} \equiv -2(\theta_2 + \theta_5) = \bar{\phi}_1 + \beta_1 \\ \tilde{\theta}_{2,n} \equiv -2(\theta_2 + \theta_1) = \bar{\phi}_2 + \beta_2, \\ \tilde{\theta}_{3,n} \equiv -2(\theta_1 + \theta_5) = \bar{\phi}_3 + \beta_3 \end{cases} \tag{37}$$

where each β_j is either $\pi/2$ or $-\pi/2$. Making these selections fixes the following values

$$\begin{cases} 2(\theta_2 - \theta_5) = -\bar{\phi}_2 + \bar{\phi}_3 + \beta_3 - \beta_2 \\ 2(\theta_5 - \theta_1) = -\bar{\phi}_1 + \bar{\phi}_2 + \beta_2 - \beta_1 \\ 2(\theta_2 - \theta_1) = -\bar{\phi}_1 + \bar{\phi}_3 + \beta_3 - \beta_1 \end{cases}. \tag{38}$$

Since the combinations of β_j appearing in equation (38) yield either $\pm\pi$ or 0, we choose the β-parameters in a way that we alternate between these values to marginalise over the value c_i appearing in each of the three likelihoods. This yields a likelihood equivalent to equation (33) for the measurement of each stabiliser. For the selection given by equation (37) it is guaranteed that our protocol realises adaptive optimal measurements with a scaling of the variance of the estimated phases given by $\sigma^2_{i,n} = 4/n$. A pseudocode that summarises the steps presented here is shown in figure 8. Additionally, the discussed protocol has the benefit that in each measurement one can use the value of all three stabilisers as opposed to the PHOM and the Bayesian inference with the constant cosine, for which each measurement only yields information about the scanned stabiliser currently under consideration. Thus, the estimate of each phase will still have a variance σ^2_n given by

$$\sigma^2_n = \frac{4}{n}. \tag{39}$$

Finally, it is interesting to analyse by how much the efficiency of the protocol would decrease if one did not make an adaptive choice of the parameters. If one selected the values $\tilde{\theta}_{i,n}$ randomly, then $\alpha_{i,n}$ would have a mean value equal to $\overline{\alpha}_{i,n} = (2 - \sqrt{3})/2 \approx 0.134$, which is readily obtained by integrating equation (36) over a uniform probability distribution of $\tilde{\theta}_{i,n}$. Taking into consideration equation (14) the scaling of the variance in such a non-adaptive protocol would be given by

$$\sigma^2_{i,n} \approx \frac{1}{0.134n} \approx \frac{7.5}{n}. \tag{40}$$

Thus, adaptive optimal selection of parameters in our protocol reduces the number of measurements needed by almost a factor of two.

5. Three-plaquette case

The methods seen in the previous sections can be generalised to the more complex case of the entire seven-qubit code. In this case the objective is to measure the 7 phases that can appear in the preparation of the state that represents the logical state $|0\rangle_L$ (see appendix A). To this end, we can measure seven different combinations of stabilisers: $S_x^{(1)}$, $S_x^{(2)}$, $S_x^{(3)}$, $S_x^{(1)}S_x^{(2)}$, $S_x^{(1)}S_x^{(3)}$, $S_x^{(2)}S_x^{(3)}$ and $S_x^{(1)}S_x^{(2)}S_x^{(3)}$. The marginal likelihood for the measurement of the first stabiliser is

Input: n copies of the state $|\psi'\rangle$
Output: List of estimated phases $\bar{\boldsymbol{\phi}} = \{\bar{\phi}_1, \bar{\phi}_2, \bar{\phi}_3\}$
and corresponding probability distributions $\mathcal{P} = \{P(\phi_1), P(\phi_2), P(\phi_3)\}$
• Define
$\boldsymbol{\theta} = \{\theta_1, \theta_2, \theta_5\}$ ▹ angles θ_k to perform rotations on qubit k
$\Pi = \{P_2(\pm_{\boldsymbol{\theta}}, \phi_1), P_1(\pm_{\boldsymbol{\theta}}, \phi_2), P_{12}(\pm_{\boldsymbol{\theta}}, \phi_3)\}$ ▹ likelihoods corresponding to ϕ_1, ϕ_2, ϕ_3
$\mathcal{S} = \{S_x^{(2)}, S_x^{(1)}, S_x^{(1)}S_x^{(2)}\}$ ▹ stabilizers corresponding to the likelihoods Π
• Set all probability distributions in $\mathcal{P}$ equal to $1/2\pi$
• Set all the angles in $\boldsymbol{\theta}$ equal to zero
for m **in** n **do**
• Rotate qubits $\mathcal{Q} = \{1, 2, 5\}$ along the Z axis by the angles in $\boldsymbol{\theta}$
• Measure the stabilizers in $\mathcal{S}$ and obtain the measurement set $\mathcal{M}$
for j in $J = 1, 2, 3$ **do** ▹ The set J corresponds to the indices of the phases in $\bar{\boldsymbol{\phi}}$
• Update the j-th probability in $\mathcal{P}$ with the j-th likelihood in Π according to the j-th measurement in $\mathcal{M}$
• Compute the maximum of the j-th probability in $\mathcal{P}$ and denote it as $\bar{\phi}_j$
• Update the list of estimated phases with $\bar{\phi}_j$
end for
• Compute the new rotation angles in $\boldsymbol{\theta}$ by solving the linear system S

$$S = \begin{cases} 2(\theta_2 + \theta_5) = -\bar{\phi}_1 + \beta_1 \\ 2(\theta_2 + \theta_1) = -\bar{\phi}_2 + \beta_2 \\ 2(\theta_1 + \theta_5) = -\bar{\phi}_3 + \beta_3 \end{cases}$$

where each β_j is chosen alternately at each measurement between $\{+\pi/2, -\pi/2\}$
end for

Figure 8. Pseudocode to determine the three phases, $\boldsymbol{\phi} = \{\phi_1, \phi_2, \phi_3\}$, appearing in the two-plaquette case of section 4 by implementation of the marginal likelihood Bayesian inference method. This pseudocode can also be applied for estimating the seven phases appearing in the three-plaquette case of section 5 after redefining $\boldsymbol{\phi}$, the list of unknown phases and their indices J; $\mathcal{P}$, their probability distributions; $\boldsymbol{\theta}$, the angles for the rotations of the measurements; Π, the likelihoods; $\mathcal{S}$ the list of stabilisers; $\mathcal{Q}$ the list of qubits to be rotated; the system of equations S according to (A.20) in appendix A.

$$P_1(\pm_{\boldsymbol{\theta}}|\phi_2) = \frac{4 \pm \cos(\phi_2 - \tilde{\theta}_2)}{8}, \tag{41}$$

where $\tilde{\theta}_2 \equiv -2(\theta_1 + \theta_2 + \theta_3 + \theta_4)$. Similar expressions are obtained for the other six combinations of stabilisers (see appendix A). Following the same process as in the previous sections, the behaviour of the variance and the values of α for each angle ϕ_i at the step n ($\alpha_{i,n}$) are now given by (see appendix B)

$$\overline{\sigma_{i,n+1}^2 - \sigma_{i,n}^2} = -\alpha_{i,n}\sigma_{i,n}^4, \tag{42}$$

with

$$\alpha_{i,n} = \frac{e^{\sigma_{i,n}^2}\sin^2(\overline{\phi}_{i,n} - \tilde{\theta}_{i,n})}{16 - e^{\sigma_{i,n}^2}\cos^2(\overline{\phi}_{i,n} - \tilde{\theta}_{i,n})}, \tag{43}$$

where for small values of $\sigma_{i,n}^2$ one finds

$$\alpha_{i,n} \approx \frac{\sin^2(\overline{\phi}_{i,n} - \tilde{\theta}_{i,n})}{16 - \cos^2(\overline{\phi}_{i,n} - \tilde{\theta}_{i,n})}. \tag{44}$$

The maximum value of each $\alpha_{i,n}$ is $1/16$ for the selection $\tilde{\theta}_{i,n} = \bar{\phi}_{i,n} \pm \pi/2$. Thus, this rule ensures an adaptive way of selecting the measurements that yields more information than a non-adaptive selection and gives a scaling as

$$\sigma_n^2 = \frac{16}{n} \tag{45}$$

for the variance of the estimate for each phase measured.

5.1. PHOM simulations

In this section we discuss numerical simulations to obtain the behaviour of the variances for the PHOM with the number of measurements used in the three-plaquette case.

We initially fix the number of iterations I to be performed as explained in step (iv) of section 4.1 and we choose a number n of copies of the initial quantum state that we can measure. We then choose $\mathcal{N}$ different seven-dimensional

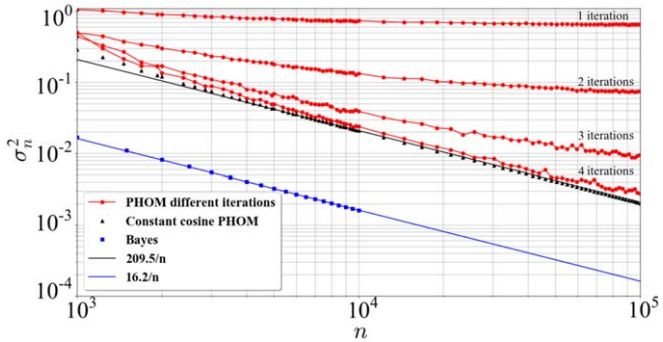

Figure 9. Behaviour of the variance as a function of the total number of measurements n. Only for the PHOM, the total number of measurements is given by $n = 7 \cdot M \cdot I \cdot$ mpp, where 7 corresponds to the number of phases to be estimated, M is the number of divisions of the interval $[-\pi, \pi]$ of each phase, I is the number of iterations used for the PHOM, and mpp is the number of measurements for each of the M divisions. For the PHOM using constant cosines a behaviour of $\sigma_n^2 = (209.5 \pm 0.5)/n$ is obtained. The PHOM shows a similar behaviour when using enough iterations for the method to converge. Finally, using marginal Bayes the performance is $\sigma_n^2 = (16.2 \pm 0.1)/n$. Error bars for results of the constant cosine PHOM and the Bayes method are smaller than the symbol size.

vectors representing the seven initially unknown phases $\boldsymbol{\phi}^{(k)}$ ($k = 1,\ldots,\mathcal{N}$). We perform the PHOM following section 4.1 and the expressions (A.4)–(A.11) in appendix A in order to obtain an estimate of the seven phases $\boldsymbol{\phi}_{\text{est}}^{(k)}$. For each of the vectors, we calculate the difference between the estimated phases and the phases chosen initially: $\boldsymbol{\phi}_{\text{est}}^{(k)} - \boldsymbol{\phi}^{(k)}$. We finally compute an estimate of the variance of the PHOM for a given n and a fixed number of iterations I as

$$\sigma_n^2 = \frac{1}{\mathcal{N}} \sum_{k=1}^{\mathcal{N}} (\boldsymbol{\phi}_{\text{est}}^{(k)} - \boldsymbol{\phi}^{(k)})^2, \tag{46}$$

where $\mathcal{N}$ is a large number to obtain a good estimate of σ_n^2, in our case $\mathcal{N} = 50\,000$. To perform the scans of each stabiliser we divide the intervals $[-\pi, \pi]$ of the angles θs into $M = 10$ points. Since we have to measure seven stabilisers, the number of measurements per point we can perform is $\text{mpp} = n/(7MI)$.

Repeating this process using a different n and $I = 1,\ldots,4$ yields the data plotted with circles in figure 9. A similar process is done for the constant cosine PHOM without performing iterations since they are not needed for this method (see section 4.1). The results obtained for this case are represented by the triangles in figure 9. It can be seen that as the number of iterations used for the PHOM increases, the variance with the number of resources decreases until reaching a similar behaviour as that of the constant cosine PHOM. The reason for this is that the PHOM has two limitations, one given by the number of iterations and another by the finite number of measurements used for each scan. If a small number of iterations is used, most of the PHOM simulations do not converge and the result is a wrong estimation for the phases which results in a big variance. As the number of iterations increases, more simulations converge to a correct phase and the variance obtained decreases. After performing enough iterations, all the simulations converge and the only source of error is the number of measurements used for each scan. As this number increases, the statistical error of each scan performed decreases yielding a better estimate of each phase. This behaviour is represented in figure 10.

Performing a fit of the relation between the variance and the number of measurements for the constant cosine PHOM yields a behaviour of $\sigma_n^2 = (209.5 \pm 0.5)/n$.

5.2. Marginal likelihood Bayes simulations

To obtain the behaviour of the variance with the number of measurements for the marginal likelihood Bayes inference method we apply a generalisation of the method shown in the pseudocode of figure 8 with the expressions (A.12)–(A.20) in appendix A. After performing enough measurements ($\approx$100) the probability distribution obtained can be approximated by a normal probability distribution for each of the phases that is used for computing the variances and for estimating the error of this adaptive technique. The results for the variances are shown in figure 9 where the data is plotted with squares. It can be seen that the variance decreases as the number of measurements used increases. A numerical fit of the data obtained reveals that the variance decreases as $\sigma_n^2 = (16.2 \pm 0.1)/n$, as was expected from the analytical derivation of the method in section 5.

6. Conclusions and outlook

In this work, we have introduced an adaptive Bayesian method to measure systematic phase shift errors appearing in the experimental preparation of multi-qubit states, in particular, we have used it for correcting the errors appearing in the logical states of the Steane code. This method is capable of finding the experimental

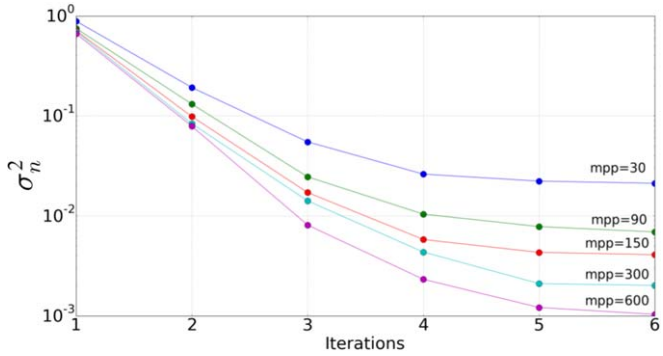

Figure 10. Behaviour of the variance for increased number of iterations of the PHOM algorithm. In each iteration the mean values of each stabiliser combination are reconstructed by performing a scan measuring an interval of length π divided in ten points and performing a fixed amount of measurements per point (mpp) for each of these divisions. The variance approaches a constant value after several iterations. This is due to the finite number of mpp introducing a constant statistical noise. As the number of mpp increases this noise decreases.

	PHOM	PHOM constant cosine	BAYES marginal likelihood
Variance σ^2	$\sim 224/n$	$(209.5 \pm 0.5)/n$	$(16.2 \pm 0.1)/n$
Efficiency relative to PHOM	1	~1	~13

Figure 11. Comparison of the efficiencies among the different methods studied to measure phases for the three-plaquette case. For the PHOM case the results for the optimal selection of iterations have been used.

configuration that optimises the information gained by each measurement performed. An analytical development of this method that yields a simple rule for this adaptive selection has been shown, thus saving computational power that would be otherwise used in finding numerically the optimal measurement at each step of the process.

We compared our method to the PHOM, a non-adaptive phase estimation method based on a generalisation of a Ramsey experiment for multi-qubit states that was recently realised for the implementation of the Steane code [26]. We simulated both of them to measure quantum phases appearing in the preparation of quantum states needed for the Steane code. The efficiency obtained by simulation of our method is in agreement with the efficiency derived from the theoretical calculations, and shows an improvement by a reduction of the required measurement time by more than one order of magnitude when compared with the efficiency of the PHOM (see figure 11). We notice that although there are methods that yield a better efficiency than the SQL [8, 46–48], these methods rely on the non-trivial implementation of multi-qubit gates which we do not consider here. However, it might be interesting to analyse generalisations of our protocol by using these kind of techniques.

Furthermore, the method, illustrated for the optimisation of the seven-qubit Steane code, is applicable to other QEC codes and stabiliser states. Additionally, since this method only relies on the application of single-qubit rotations and measurements, it can correct systematic errors appearing in multi-qubit states implemented in different physical platforms. Thus, it has potential application in a variety of systems for quantum information processing such as, e.g. trapped ions, Rydberg atoms in optical lattices or tweezer arrays or other AMO or solid-state architectures.

Acknowledgments

We thank P Schindler for useful discussions. We acknowledge support by US ARO through Grant No. W911NF-14-1-010. MM acknowledges support from the AQTION project (820495), funded by the European Union Quantum Technology Flagship. The research is also based upon work supported by the Office of the Director of National Intelligence (ODNI), Intelligence Advanced Research Projects Activity (IARPA), via the US Army Research Office Grant No. W911NF-16-1-0070. The views and conclusions contained herein are those of the authors and should not be interpreted as necessarily representing the official policies or endorsements, either expressed or implied, of the ODNI, IARPA, or the US Government. The US Government is authorised to

reproduce and distribute reprints for Governmental purposes notwithstanding any copyright annotation thereon. Any opinions, findings, and conclusions or recommendations expressed in this material are those of the author(s) and do not necessarily reflect the view of the US Army Research Office. Numerical simulations have been performed on the Swansea SUNBIRD system. The Swansea SUNBIRD system is part of the Supercomputing Wales project, which is part-funded by the European Regional Development Fund (ERDF) via Welsh Government.

Appendix A. Three-plaquette case: quantum states, likelihoods and pseudocode generalisation

In this appendix we provide details on the expressions appearing in the three-plaquette case. For the seven-qubit Steane code the logical 0 is given by

$$|0\rangle_L = \frac{1}{2\sqrt{2}}(|0000000\rangle + |0110110\rangle + |1111000\rangle + |1001110\rangle + |0011011\rangle + |0101101\rangle + |1100011\rangle + |1010101\rangle). \tag{A.1}$$

Due to experimental errors, phases appear in the preparation of the $|0\rangle_L$ state. The state obtained will be then

$$|0'\rangle_L = \frac{1}{2\sqrt{2}}(|0000000\rangle + e^{i\phi_1}|0110110\rangle + e^{i\phi_2}|1111000\rangle + e^{i\phi_3}|1001110\rangle + e^{i\phi_4}|0011011\rangle + e^{i\phi_5}|0101101\rangle + e^{i\phi_6}|1100011\rangle + e^{i\phi_7}|1010101\rangle). \tag{A.2}$$

Single-qubit Z rotations can be performed on the seven qubits of the code state $|0'\rangle_L$ to obtain the following state and likelihoods for each stabiliser combination

$$\begin{aligned}|0'\rangle_L \xrightarrow{\text{Rotations}} \frac{1}{2\sqrt{2}}(&|0000000\rangle + e^{i[\phi_1+2(\theta_2+\theta_3+\theta_5+\theta_6)]}|0110110\rangle \\ &+ e^{i[\phi_2+2(\theta_1+\theta_2+\theta_3+\theta_4)]}|1111000\rangle + e^{i[\phi_3+2(\theta_1+\theta_4+\theta_5+\theta_6)]}|1001110\rangle \\ &+ e^{i[\phi_4+2(\theta_3+\theta_4+\theta_6+\theta_7)]}|0011011\rangle + e^{i[\phi_5+2(\theta_2+\theta_4+\theta_5+\theta_7)]}|0101101\rangle \\ &+ e^{i[\phi_6+2(\theta_1+\theta_2+\theta_6+\theta_7)]}|1100011\rangle + e^{i[\phi_7+2(\theta_1+\theta_3+\theta_5+\theta_7)]}|1010101\rangle),\end{aligned} \tag{A.3}$$

$$\begin{aligned}P_1(\pm_{\boldsymbol{\theta}}|\boldsymbol{\phi}) = \frac{1}{8}\{&4 \pm \cos[\phi_2 + 2(\theta_1 + \theta_2 + \theta_3 + \theta_4)] \pm \cos[\phi_1 - \phi_3 + 2(-\theta_1 + \theta_2 + \theta_3 - \theta_4)] \\ &\pm \cos[\phi_4 - \phi_6 + 2(-\theta_1 - \theta_2 + \theta_3 + \theta_4)] \pm \cos[\phi_5 - \phi_7 + 2(-\theta_1 + \theta_2 - \theta_3 + \theta_4)]\},\end{aligned} \tag{A.4}$$

$$\begin{aligned}P_2(\pm_{\boldsymbol{\theta}}|\boldsymbol{\phi}) = \frac{1}{8}\{&4 \pm \cos[\phi_1 + 2(\theta_2 + \theta_3 + \theta_5 + \theta_6)] \pm \cos[\phi_2 - \phi_3 + 2(\theta_2 + \theta_3 - \theta_5 - \theta_6)] \\ &\pm \cos[\phi_4 - \phi_5 + 2(-\theta_2 + \theta_3 - \theta_5 + \theta_6)] \pm \cos[\phi_6 - \phi_7 + 2(\theta_2 - \theta_3 - \theta_5 + \theta_6)]\},\end{aligned} \tag{A.5}$$

$$\begin{aligned}P_3(\pm_{\boldsymbol{\theta}}|\boldsymbol{\phi}) = \frac{1}{8}\{&4 \pm \cos[\phi_4 + 2(\theta_3 + \theta_4 + \theta_6 + \theta_7)] \pm \cos[\phi_1 - \phi_5 + 2(\theta_3 - \theta_4 + \theta_6 - \theta_7)] \\ &\pm \cos[\phi_2 - \phi_6 + 2(\theta_3 + \theta_4 - \theta_6 - \theta_7)] \pm \cos[\phi_3 - \phi_7 + 2(-\theta_3 + \theta_4 + \theta_6 - \theta_7)]\},\end{aligned} \tag{A.6}$$

$$\begin{aligned}P_{12}(\pm_{\boldsymbol{\theta}}|\boldsymbol{\phi}) = \frac{1}{8}\{&4 \pm \cos[\phi_3 + 2(\theta_1 + \theta_4 + \theta_5 + \theta_6)] \pm \cos[\phi_1 - \phi_2 + 2(-\theta_1 - \theta_4 + \theta_5 + \theta_6)] \\ &\pm \cos[\phi_4 - \phi_7 + 2(-\theta_1 + \theta_4 - \theta_5 + \theta_6)] \pm \cos[\phi_5 - \phi_6 + 2(-\theta_1 + \theta_4 + \theta_5 - \theta_6)]\},\end{aligned} \tag{A.7}$$

$$\begin{aligned}P_{13}(\pm_{\boldsymbol{\theta}}|\boldsymbol{\phi}) = \frac{1}{8}\{&4 \pm \cos[\phi_6 + 2(\theta_1 + \theta_2 + \theta_6 + \theta_7)] \pm \cos[\phi_1 - \phi_7 + 2(-\theta_1 + \theta_2 + \theta_6 - \theta_7)] \\ &\pm \cos[\phi_2 - \phi_4 + 2(\theta_1 + \theta_2 - \theta_6 - \theta_7)] \pm \cos[\phi_3 - \phi_5 + 2(\theta_1 - \theta_2 + \theta_6 - \theta_7)]\},\end{aligned} \tag{A.8}$$

$$\begin{aligned}P_{23}(\pm_{\boldsymbol{\theta}}|\boldsymbol{\phi}) = \frac{1}{8}\{&4 \pm \cos[\phi_5 + 2(\theta_2 + \theta_4 + \theta_5 + \theta_7)] \pm \cos[\phi_1 - \phi_4 + 2(\theta_2 - \theta_4 + \theta_5 - \theta_7)] \\ &\pm \cos[\phi_2 - \phi_7 + 2(\theta_2 + \theta_4 - \theta_5 - \theta_7)] \pm \cos[\phi_3 - \phi_6 + 2(-\theta_2 + \theta_4 + \theta_5 - \theta_7)]\},\end{aligned} \tag{A.9}$$

$$\begin{aligned}P_{123}(\pm_{\boldsymbol{\theta}}|\boldsymbol{\phi}) = \frac{1}{8}\{&4 \pm \cos[\phi_7 + 2(\theta_1 + \theta_3 + \theta_5 + \theta_7)] \pm \cos[\phi_1 - \phi_6 + 2(-\theta_1 + \theta_3 + \theta_5 - \theta_7)] \\ &\pm \cos[\phi_2 - \phi_5 + 2(\theta_1 + \theta_3 - \theta_5 - \theta_7)] \pm \cos[\phi_3 - \phi_4 + 2(\theta_1 - \theta_3 + \theta_5 - \theta_7)]\}.\end{aligned} \tag{A.10}$$

The expected values of each plaquette can be easily obtained from these expressions. For example, the first plaquette expected value is given by

$$\langle S_x^{(1)} \rangle = P_1(+\boldsymbol{\theta}|\boldsymbol{\phi}) - P_1(-\boldsymbol{\theta}|\boldsymbol{\phi}). \tag{A.11}$$

The expected values for the other plaquettes can be obtained from the corresponding likelihood in the same way. The marginal likelihoods are given by

$$P_1(\pm\boldsymbol{\theta}|\phi_2) = \frac{4 \pm \cos[\phi_2 - \tilde{\theta}_2]}{8}, \tag{A.12}$$

$$P_2(\pm\boldsymbol{\theta}|\phi_1) = \frac{4 \pm \cos[\phi_1 - \tilde{\theta}_1]}{8}, \tag{A.13}$$

$$P_3(\pm\boldsymbol{\theta}|\phi_4) = \frac{4 \pm \cos[\phi_4 - \tilde{\theta}_4]}{8}, \tag{A.14}$$

$$P_{12}(\pm\boldsymbol{\theta}|\phi_3) = \frac{4 \pm \cos[\phi_3 - \tilde{\theta}_3]}{8}, \tag{A.15}$$

$$P_{13}(\pm\boldsymbol{\theta}|\phi_6) = \frac{4 \pm \cos[\phi_6 - \tilde{\theta}_6]}{8}, \tag{A.16}$$

$$P_{23}(\pm\boldsymbol{\theta}|\phi_5) = \frac{4 \pm \cos[\phi_5 - \tilde{\theta}_5]}{8}, \tag{A.17}$$

$$P_{123}(\pm\boldsymbol{\theta}|\phi_7) = \frac{4 \pm \cos[\phi_7 - \tilde{\theta}_7]}{8}, \tag{A.18}$$

where

$$\tilde{\Theta} = \begin{cases} \tilde{\theta}_2 \equiv -2(\theta_1 + \theta_2 + \theta_3 + \theta_4) \\ \tilde{\theta}_1 \equiv -2(\theta_2 + \theta_3 + \theta_5 + \theta_6) \\ \tilde{\theta}_4 \equiv -2(\theta_3 + \theta_4 + \theta_6 + \theta_7) \\ \tilde{\theta}_3 \equiv -2(\theta_1 + \theta_4 + \theta_5 + \theta_6) \\ \tilde{\theta}_6 \equiv -2(\theta_1 + \theta_2 + \theta_6 + \theta_7) \\ \tilde{\theta}_5 \equiv -2(\theta_2 + \theta_4 + \theta_5 + \theta_7) \\ \tilde{\theta}_7 \equiv -2(\theta_1 + \theta_3 + \theta_5 + \theta_7) \end{cases}. \tag{A.19}$$

As for the generalisation of the pseudocode in figure 8, it is achieved by changing the previous definitions to the following ones

$$\begin{aligned} &J = 1,\ldots,7, \\ &S = \{\tilde{\theta}_i = \phi_i + \beta_i\}, \\ &\mathcal{Q} = \{1,\ 2,\ 3,\ 4,\ 5,\ 6,\ 7\}, \\ &\mathcal{T} = \{\theta_1,\ \theta_2,\ \theta_3,\ \theta_4,\ \theta_5,\ \theta_6,\ \theta_7\}, \\ &\boldsymbol{\phi} = \{\phi_1,\ \phi_2,\ \phi_3,\ \phi_4,\ \phi_5,\ \phi_6,\ \phi_7\}, \\ &\mathcal{P} = \{P(\phi_1),\ P(\phi_2),\ P(\phi_3),\ P(\phi_4),\ P(\phi_5),\ P(\phi_6),\ P(\phi_7)\}, \\ &\mathcal{S} = \{S_x^{(2)},\ S_x^{(1)},\ S_x^{(1)}S_x^{(2)},\ S_x^{(3)},\ S_x^{(2)}S_x^{(3)},\ S_x^{(1)}S_x^{(3)},\ S_x^{(1)}S_x^{(2)}S_x^{(3)}\}, \\ &\Pi = \{P_2(\pm\boldsymbol{\theta}|\phi_1),\ P_1(\pm\boldsymbol{\theta}|\phi_2),\ P_{12}(\pm\boldsymbol{\theta}|\phi_3),\ P_3(\pm\boldsymbol{\theta}|\phi_4),\ P_{23}(\pm\boldsymbol{\theta}|\phi_5),\ P_{13}(\pm\boldsymbol{\theta}|\phi_6),\ P_{123}(\pm\boldsymbol{\theta}|\phi_7)\}, \end{aligned} \tag{A.20}$$

where the β_i in S are chosen randomly from the set $\{+\pi/2,\ -\pi/2\}$.

Appendix B. Analytical study of the scaling of the variance

In this appendix, we present some details on the scaling of the variance with the number of measurements when applying the Bayesian adaptive method to the single-qubit state of equation (1). The expressions obtained are easy to generalise to the two and three-plaquette cases. Let us suppose after n measurements the knowledge about the phase ϕ is given by a normal distribution with mean value $\overline{\phi}_n$ and variance σ_n^2

$$P_n(\phi) = \frac{1}{\sqrt{2\pi\sigma_n^2}} \mathrm{e}^{-\frac{(\phi-\overline{\phi}_n)^2}{2\sigma_n^2}}. \tag{B.1}$$

After performing a measurement the updated probability distribution is given by

$$P_{n+1}^{\pm}(\phi) = \frac{1}{p_n^{\pm}} \left(\frac{1 \pm \cos(\phi - \theta_n)}{2} \right) P_n(\phi), \tag{B.2}$$

where $p_n^{\pm}$ is the probability at step n of obtaining a $+$ or $-$ in the measurement $n+1$. Since at step n it is unknown what the measurement $n+1$ will yield, we consider the expected value of the variance after the measurement $n+1$, $\overline{\sigma^2}_{n+1}$

$$\overline{\sigma^2}_{n+1} = p_n^{+}(\sigma_{n+1}^{+})^2 + p_n^{-}(\sigma_{n+1}^{-})^2, \tag{B.3}$$

where $(\sigma_{n+1}^{\pm})^2$ are the variances after obtaining a $+$ or $-$ for the measurement $n+1$ given by

$$(\sigma^{\pm}{}_{n+1})^2 = \int_{-\pi}^{\pi} \phi^2 P_{n+1}^{\pm}(\phi)\mathrm{d}\phi - \left(\int_{-\pi}^{\pi} \phi P_{n+1}^{\pm}(\phi)\mathrm{d}\phi\right)^2. \tag{B.4}$$

This yields

$$p_n^{+}(\sigma_{n+1}^{+})^2 = \int_{-\pi}^{\pi} \phi^2 P_n(\phi)\frac{1+\cos(\phi-\theta_n)}{2}\mathrm{d}\phi - \frac{1}{p_n^{+}}\left(\int_{-\pi}^{\pi} \phi P_n(\phi)\frac{1+\cos(\phi-\theta_n)}{2}\mathrm{d}\phi\right)^2, \tag{B.5}$$

$$p_n^{-}(\sigma_{n+1}^{-})^2 = \int_{-\pi}^{\pi} \phi^2 P_n(\phi)\frac{1-\cos(\phi-\theta_n)}{2}\mathrm{d}\phi - \frac{1}{p_n^{+}}\left(\int_{-\pi}^{\pi} \phi P_n(\phi)\frac{1-\cos(\phi-\theta_n)}{2}\mathrm{d}\phi\right)^2. \tag{B.6}$$

Introducing (B.5) and (B.6) into (B.3) yields

$$\begin{aligned}\overline{\sigma^2}_{n+1} = \sigma_n^2 - \frac{1}{4p_n^{+}p_n^{-}}\left(\int_{-\pi}^{\pi} \phi P_n(\phi)\cos(\phi-\theta_n)\mathrm{d}\phi\right)^2 + \frac{p_n^{+}-p_n^{-}}{2p_n^{+}p_n^{-}}\left(\int_{-\pi}^{\pi} \phi P_n(\phi)\mathrm{d}\phi\right)\\ \times\left(\int_{-\pi}^{\pi} \phi P_n(\phi)\cos(\phi-\theta_n)\mathrm{d}\phi\right) + \frac{4p_n^{+}p_n^{-}-1}{4p_n^{+}p_n^{-}}\left(\int_{-\pi}^{\pi} \phi P_n(\phi)\mathrm{d}\phi\right)^2,\end{aligned} \tag{B.7}$$

where

$$4p_n^{+}p_n^{-}-1 = -\left(\int_{-\pi}^{\pi} P_n(\phi)\cos(\phi-\theta_n)\mathrm{d}\phi\right)^2, \tag{B.8}$$

$$p_n^{+}-p_n^{-} = \left(\int_{-\pi}^{\pi} P_n(\phi)\cos(\phi-\theta_n)\mathrm{d}\phi\right). \tag{B.9}$$

Thus, we obtain

$$\begin{aligned}\overline{\sigma^2{}_{n+1}-\sigma^2{}_n} = -\frac{1}{p^{+}p^{-}}\left[\left(\int_{-\pi}^{\pi} \frac{P_n(\phi)\cos(\phi-\theta_n)}{2}\mathrm{d}\phi\right)\right.\\ \left.\times\left(\int_{-\pi}^{\pi} \phi P_n(\phi)\mathrm{d}\phi\right) - \left(\int_{-\pi}^{\pi} \frac{\phi P_n(\phi)\cos(\phi-\theta_n)}{2}\mathrm{d}\phi\right)\right]^2.\end{aligned} \tag{B.10}$$

If we consider $P_n(\phi)$ has a low standard deviation we can change the intervals of integration $[-\pi,\pi)$ with $(-\infty,\infty)$ to obtain

$$\begin{aligned}&\int_{-\infty}^{\infty} \phi P_n(\phi)\mathrm{d}\phi = \overline{\phi}_n,\\ &\int_{-\infty}^{\infty} \frac{P_n(\phi)\cos(\phi-\theta_n)}{2}\mathrm{d}\phi = \frac{\mathrm{e}^{-\sigma_n^2/2}}{2}\cos(\overline{\phi}_n-\theta_n),\\ &\int_{-\infty}^{\infty} \frac{\phi P_n(\phi)\cos(\phi-\theta_n)}{2}\mathrm{d}\phi = -\frac{\mathrm{e}^{-\sigma_n^2/2}\sigma_n^2}{2}\sin(\overline{\phi}_n-\theta_n) + \frac{\mathrm{e}^{-\sigma_n^2/2}\overline{\phi}_n}{2}\cos(\overline{\phi}_n-\theta_n),\\ &p^{\pm} = \frac{1}{2}(1\pm\mathrm{e}^{-\sigma_n^2/2}\cos(\overline{\phi}_n-\theta_n).\end{aligned} \tag{B.11}$$

Replacing the values of these integrals in (B.10) we obtain

$$\overline{\sigma^2{}_{n+1}-\sigma^2{}_n} = -\frac{\mathrm{e}^{-\sigma_n^2}\sigma_n^4\sin^2(\overline{\phi}_n-\theta_n)}{1-\mathrm{e}^{-\sigma_n^2}\cos^2(\overline{\phi}_n-\theta_n)}. \tag{B.12}$$

Similar calculations can be performed for the two and three plaquette case likelihoods, the only difference being the cosine appearing in the likelihood having amplitude $1/4$ and $1/8$ respectively and the angle $\tilde{\theta}_{i,n}$ being a linear combination of the rotations performed on different qubits at the step n. Taking this into account, for the two plaquette case the decrease in the variance for each ϕ_i is

$$\overline{\sigma^2{}_{i,n+1}-\sigma^2{}_{i,n}} = -\frac{\mathrm{e}^{-\sigma_{i,n}^2}\sigma_{i,n}^4\sin^2(\overline{\phi}_{i,n}-\theta_{i,n})}{4-\mathrm{e}^{-\sigma_{i,n}^2}\cos^2(\overline{\phi}_{i,n}-\theta_{i,n})} \tag{B.13}$$

and for the three plaquette case

$$\overline{\sigma^2{}_{i,n+1} - \sigma^2{}_{i,n}} = -\frac{e^{-\sigma^2_{i,n}}\sigma^4_{i,n}\sin^2(\overline{\phi}_{i,n} - \theta_{i,n})}{16 - e^{-\sigma^2_{i,n}}\cos^2(\overline{\phi}_{i,n} - \theta_{i,n})}. \tag{B.14}$$

ORCID iDs

F Martínez-García https://orcid.org/0000-0001-7243-3663
D Vodola https://orcid.org/0000-0003-0880-3548
M Müller https://orcid.org/0000-0002-2813-3097

References

[1] Nielsen M A and Chuang I 2002 *Quantum Computation and Quantum Information* (Cambridge: Cambridge University Press)
[2] DiVincenzo D P 2000 *Fortschr. Phys.: Progress Phys.* **48** 771–83
[3] Terhal B M 2015 *Rev. Mod. Phys.* **87** 307
[4] Breuer H P and Petruccione F 2002 *The Theory of Open Quantum Systems* (Oxford: Oxford University Press)
[5] Ramsey N F 1950 *Phys. Rev.* **78** 695
[6] Foot C J 2005 *Atomic Physics* (Oxford: Oxford University Press)
[7] Huszár F and Houlsby N M 2012 *Phys. Rev.* A **85** 052120
[8] Wiebe N and Granade C 2016 *Phys. Rev. Lett.* **117** 010503
[9] Granade C, Ferrie C and Flammia S T 2017 *New J. Phys.* **19** 113017
[10] Sugiyama T, Turner P S and Murao M 2012 *Phys. Rev.* A **85** 052107
[11] Fischer D G, Kienle S H and Freyberger M 2000 *Phys. Rev.* A **61** 032306
[12] Kravtsov K, Straupe S, Radchenko I, Houlsby N, Huszár F and Kulik S 2013 *Phys. Rev.* A **87** 062122
[13] Mahler D, Rozema L A, Darabi A, Ferrie C, Blume-Kohout R and Steinberg A 2013 *Phys. Rev. Lett.* **111** 183601
[14] Granade C E, Ferrie C, Wiebe N and Cory D G 2012 *New J. Phys.* **14** 103013
[15] Shlyakhov A R, Zemlyanov V V, Suslov M V, Lebedev A V, Paraoanu G S, Lesovik G B and Blatter G 2018 *Phys. Rev.* A **97** 022115
[16] Lidar D A and Brun T A 2013 *Quantum Error Correction* (Cambridge: Cambridge University Press)
[17] Cramer M, Plenio M B, Flammia S T, Somma R, Gross D, Bartlett S D, Landon-Cardinal O, Poulin D and Liu Y K 2010 *Nat. Commun.* **1** 149
[18] Müller M, Rivas A, Martínez E, Nigg D, Schindler P, Monz T, Blatt R and Martin-Delgado M 2016 *Phys. Rev.* X **6** 031030
[19] Steane A M 1996 *Phys. Rev. Lett.* **77** 793
[20] Häffner H, Roos C F and Blatt R 2008 *Phys. Rep.* **469** 155–203
[21] Leibfried D, Blatt R, Monroe C and Wineland D 2003 *Rev. Mod. Phys.* **75** 281
[22] Brown K R, Kim J and Monroe C 2016 *npj Quantum Inf.* **2** 16034
[23] Blatt R and Wineland D 2008 *Nature* **453** 1008
[24] Blinov B B, Leibfried D, Monroe C and Wineland D J 2004 *Quantum Inf. Process.* **3** 45–59
[25] Harty T P, Allcock D T C, Ballance C J, Guidoni L, Janacek H A, Linke N M, Stacey D N and Lucas D M 2014 *Phys. Rev. Lett.* **113** 220501
[26] Nigg D, Müller M, Martinez E A, Schindler P, Hennrich M, Monz T, Martin-Delgado M A and Blatt R 2014 *Science* **345** 302
[27] Sriarunothai T, Wölk S, Giri G S, Friis N, Dunjko V, Briegel H J and Wunderlich C 2018 *Quantum Sci. Technol.* **4** 015014
[28] Johanning M, Varón A F and Wunderlich C 2009 *J. Phys. B: At. Mol. Opt. Phys.* **42** 154009
[29] Jaksch D, Cirac J, Zoller P, Rolston S, Côté R and Lukin M 2000 *Phys. Rev. Lett.* **85** 2208
[30] Saffman M, Walker T G and Mølmer K 2010 *Rev. Mod. Phys.* **82** 2313
[31] Crow D, Joynt R and Saffman M 2016 *Phys. Rev. Lett.* **117** 130503
[32] Anderson S E, Younge K and Raithel G 2011 *Phys. Rev. Lett.* **107** 263001
[33] Viteau M, Bason M, Radogostowicz J, Malossi N, Ciampini D, Morsch O and Arimondo E 2011 *Phys. Rev. Lett.* **107** 060402
[34] Schauß P, Cheneau M, Endres M, Fukuhara T, Hild S, Omran A, Pohl T, Gross C, Kuhr S and Bloch I 2012 *Nature* **491** 87
[35] Nogrette F, Labuhn H, Ravets S, Barredo D, Béguin L, Vernier A, Lahaye T and Browaeys A 2014 *Phys. Rev.* X **4** 021034
[36] Xia T, Lichtman M, Maller K, Carr A, Piotrowicz M, Isenhower L and Saffman M 2015 *Phys. Rev. Lett.* **114** 100503
[37] Hanson R and Awschalom D D 2008 *Nature* **453** 1043
[38] Córcoles A D, Magesan E, Srinivasan S J, Cross A W, Steffen M, Gambetta J M and Chow J M 2015 *Nat. Commun.* **6** 6979
[39] Gambetta J M, Chow J M and Steffen M 2017 *npj Quantum Inf.* **3** 2
[40] Kelly J *et al* 2015 *Nature* **519** 66
[41] Waldherr G *et al* 2014 *Nature* **506** 204
[42] Fedorov A, Steffen L, Baur M, da Silva M P and Wallraff A 2012 *Nature* **481** 170
[43] Press W H, Teukolsky S A, Vetterling W T and Flannery B P 2007 *Numerical Recipes III Edition: The Art of Scientific Computing* (Cambridge: Cambridge University Press)
[44] Negnevitsky V 2018 Feedback-stabilised quantum states in a mixed-species ion system *PhD Thesis* ETH Zurich
[45] Bombin H and Martin-Delgado M A 2006 *Phys. Rev. Lett.* **97** 180501
[46] Higgins B L, Berry D W, Bartlett S D, Wiseman H M and Pryde G J 2007 *Nature* **450** 393
[47] Giovannetti V, Lloyd S and Maccone L 2004 *Science* **306** 1330–6
[48] Paesani S, Gentile A A, Santagati R, Wang J, Wiebe N, Tew D P, O'Brien J L and Thompson M G 2017 *Phys. Rev. Lett.* **118** 100503